Journal of the Meteorological Society of Japan

EARLY ONLINE RELEASE

The DOI for this manuscript is
DOI:10.2151/jmsj.2022-034
J-STAGE Advance published date: April 26th, 2022
The final manuscript after publication will replace the preliminary version at the above DOI once it is available.

Investigation of characteristics of maximum storm surges in Japanese coastal regions caused by Typhoon Jebi (2018) based on typhoon track ensemble simulations

Toshikazu OTAKI

Graduate school of Education
Yokohama National University, Yokohama, Japan

Hironori FUDEYASU

Yokohama National University, Yokohama, Japan

Nadao KOHNO

Meteorological Research Institute,
Japan Meteorological Agency, Tsukuba, Japan

Tetsuya TAKEMI

Disaster Prevention Research Institute,
Kyoto University, Kyoto, Japan

Nobuhito MORI

Disaster Prevention Research Institute,
Kyoto University, Kyoto, Japan

and

Koki IIDA

Graduate school of Education
Yokohama National University, Yokohama, Japan

----

1) Corresponding author: Hironori Fudeyasu, Faculty of Education, Yokohama National University, 79-2 Tokiwadai, Hodogaya-ku, Yokohama, 240-8501, JAPAN
E-mail: fude@ynu.ac.jp Tel: +81-45-339-3346 Fax: 81-45-339-3346
2) Present affiliation of Toshikazu Otaki: IDEA Consultants, Inc., Tokyo, Japan

Abstract

The maximum storm surges caused by Typhoon Jebi (2018) were examined using a storm surge model, and by track ensemble simulations based on a meteorological model and a parametric tropical cyclone (TC) model. The storm surge at Osaka Port was estimated more accurately by the meteorological model than the parametric TC model. The differences between both models were due to a “wind setup effect,” where the topography enhanced surface winds over Osaka Bay. The typhoon track ensemble simulations demonstrated that the maximum storm surge was dependent on perturbation of the track of Typhoon Jebi along the entire coast of the Japanese Islands, including the main island, Kyushu, and Shikoku. Open shallow bays had maximum storm surges exceeding 2.50 m. In coastal areas where larger maximum storm surges were estimated, the longitudinally perturbed “worst-case course” appeared 0.4–0.8° west or east of the “hit course,” indicating that the wind setup effect was an important factor in the maximum storm surge. The distance of the worst-case course from the hit course was almost the same as the radius of maximum wind of Typhoon Jebi. Although the models had similar worst-case courses for each coastal area, the meteorological model estimated a slightly higher simulated maximum storm surge than the parametric TC model. For the main island, Kyushu, and Shikoku, approximately 6% of the maximum storm surges exceeded 2.00 m. Although these values may differ for other typhoons and sampling points, it is important to estimate the maximum storm surges and

worst-case courses at all coastal areas, including regions where storm surges by typhoons is unknown yet occurred because this will provide important information enabling effective disaster prevention and risk management.

Keywords Typhoon Jebi; maximum storm surges; typhoon-track ensemble simulation;

1. Introduction

Typhoon Jebi passed over the Shikoku and Kinki districts of Japan in early September 2018. It was accompanied by extreme winds, which caused severe damage to urban centers (e.g., Takemi et al., 2019; Takabatake et al., 2018). Low pressure and strong winds, with maximum gusts of 58.1 $m \cdot s^{-1}$ at the meteorological station in Osaka led to a record-breaking maximum storm tide of 3.29 m (storm surges of 2.77 m)[1] for that city. Storm surges caused by Typhoon Jebi resulted in extensive damage to the coastal region. Although storm surges seldom occur, their impact on coastal regions can be devastating (e.g., Kohno et al., 2018, Mori et al., 2019a). Consequently, storm surges from typhoons of varying intensity must be quantitatively estimated throughout coastal regions, including in areas where storm surges have not yet occurred.

Storm surges occur due to the effects of strong onshore winds (wind setup effect) and low pressure (inverse barometer effect). To estimate the severity of storm surges, information about the surface winds and sea-level pressure associated with typhoons intensity is needed, as well as a reliable storm surge model. Typically, several methodologies are used to assess storm surge risk. The most popular approach is to simulate a historical event or use a scenario ensemble-based (i.e., storyline approach) framework (e.g., Ninomiya et al., 2017). An alternative approach is to use a large number of ensembles, such

[1]A storm surge is an anomaly from astronomical tides, while a storm tide includes astronomical tides.

as “synthetic” typhoons (e.g., Nakajo et al., 2014) or typhoons dynamically simulated by a climate model (e.g., Yasuda et al., 2014; Yang et al., 2020; Mori et al., 2019b, 2021). The key to these approaches is the selection of typhoon characteristics in parameter space, such as the central pressure, maximum wind speed, and radius of maximum wind speed. However, the influence of topography on dynamic aspects of a typhoon must also be considered.

The methods used to estimate storm surges in Mori et al. (2020) can be divided into four categories: numerical models of specific typhoons, global climate models, climatological approaches, and statistical approaches. The models used to simulate a typhoon can be subdivided into two groups: parametric tropical cyclone (TC) models and numerical weather prediction models (hereafter, meteorological models). A meteorological model is capable of more accurately simulating a typhoon.

Parametric TC models, except for the Generalized Holland Asymmetric Model (Gao et al. 2013), assume that the sea-level pressure distribution of a typhoon has an axisymmetric structure. Surface winds are estimated by the gradient wind equation with surface friction effect. One advantage of parametric TC models is that they have low computational costs. The axisymmetric sea-level pressure, which varies with typhoon parameters such as strength and size (radius of the maximum wind), can be easily reproduced by a parametric TC model. The typhoon track can be set arbitrarily, so parametric TC models are suitable for ensemble experiments. The sea level pressure is axisymmetric, but the wind distributions are asymmetric because the effect of movement is taken into account.

The asymmetric characteristics of a typhoon become important when its structure is influenced by complex topography, which is often the case in inland bays. Meteorological models can simulate a typhoon with a structure rendered asymmetric by the influence of topography and mid-latitude environments. Thuy et al. (2014) simulated storm surges due to Typhoon Kalmaegi (2014) at the Hon Dau station in Vietnam using both parametric TC and dynamical models. The dynamical model provided more accurate results, with the difference in storm surges estimated by both models being about 1 m.

Storm surges in coastal areas are affected not only by the strength and size of a typhoon, but also by the typhoon track. Therefore, ensemble experiments must be able to estimate storm surges for various typhoon tracks. For example, Shibutani et al. (2015) used a coupled model of surge, wave, and tide “SuWAT” for storm surge calculation, and a parametric TC model for simulating Typhoon Vera (1959) with various tracks. They showed a variance of about 2 m in the maximum storm surges estimated for Nagoya Port, with a longitudinal difference in the typhoon tracks of about 50 km. By Toyoda et al. (2020) the maximum storm surge caused by Typhoon Hagibis (2019) in Tokyo Bay was evaluated using a high-resolution coupled typhoon-ocean model. The method adopted was almost the same as the Typhoon Track Ensemble Simulation (T-TES) method, which was developed by Yamasaki et al. (2017). The T-TES method modulates the initial and boundary atmosphere data so that a meteorological model can be used for ensemble experiments with longitudinally perturbed typhoon tracks. If Typhoon Hagibis had passed 100 km west of the port at Tokyo, a storm surge of about 3 m might have occurred. Such a storm surge would have exceeded the historical maximum tide level.

The surface winds and sea-level pressure distributions associated with a typhoon simulated by a meteorological model are better suited to estimate the maximum storm surge along coasts. Kowaleski et al. (2020) simulated a storm surge induced by Hurricane Irma (2017) along the southeast coast of the USA using a Weather Research and Forecast (WRF) ensemble model and the advanced circulation (ADCIRC) storm surge model. Colle et al. (2015) studied storm surges by Hurricane Sandy (2012) along the northeast coast of the USA using a subset of WRF ensemble members. Although storm surges in the USA have been investigated via ensemble experiments, no study has estimated the maximum storm surges along the entire coast of Japan via ensemble experiments and a meteorological model. Recently, ensemble experiments have been limited to bays with large storm surges due to the high computational cost (e.g., Toyoda et al., 2020).

This study evaluated maximum storm surges in multiple scenarios, assuming various tracks using the storm surge model and T-TES, which used inputs from both a parametric TC model (hereafter, Para-Jebi) and a meteorological model (hereafter WRF-Jebi). The purpose of this paper is to compare the maximum storm surges derived by both models. A further aim of this study was to quantitatively investigate the possible maximum storm surges along the entire coast of Japan, including the main island, Kyushu, and Shikoku. Our ensemble experiments using the T-TES method estimate storm surges and longitudinally perturbed “worst-case courses” assuming various tracks for Typhoon Jebi in each coastal area. The reason for focusing on Typhoon Jebi is that it caused enormous damage from storm surge in recent years and had a typical track of typhoons that impact Japan. By estimating the maximum storm surge along the coast, it was possible to determine the proportion of each region at high risk of storm surges. The remainder of this paper is organized as follows. The following section briefly describes models used in our research. In Section 3, storm surges determined by Para-Jebi and WRF-Jebi are validated and the results of ensemble simulations are discussed. Maximum storm surges and worst-case courses along the entire coast of Japan, including the main island, Kyushu, and Shikoku, are estimated in this section. The main findings are summarized and discussed in the final section.

2. Methodology

This study used the T-TES method (Yamasaki et al., 2017) to conduct ensemble experiments, in which the tracks of Typhoon Jebi were varied in the longitudinal direction.

The T-TES method modulates the initial and boundary atmospheric conditions so that typhoons with different tracks can be analyzed by a meteorological model. It should be noted that the lower boundary conditions (i.e., sea surface temperature) were not modulated in this study. Simulations subsequently performed using the meteorological model can reproduce typhoons passing through the region, assuming a track shifted westward or eastward of the actual track. The T-TES method allows the original speed and direction of travel to be largely maintained throughout the typhoon’s tracks. A total of 83 tracks were created for Typhoon Jebi by T-TES, at 0.2° intervals up to 5.0° in the westward direction and 11.4° in the eastward direction. We followed the 0.2° longitudinal shift in the T-TES method to the guideline for “Storm surge inundation are map creation guide” of Ministry of Land, Infrastructure, Transport and Tourism (MLIT, 2021). The details of how to obtain longitudinal shift are explained in Yamasaki et al. (2017).

The meteorological model (WRF-Jebi) used in this study was the Weather Research and Forecasting Model version 3.6.1 (WRF; Skamarock et al., 2008). A one-way domain was nested within the parent (outer) domain. The outer domain had 220 × 215 grid points with a horizontal resolution of 15 km, while the inner domain had 601 × 541 points with a horizontal resolution of 5 km. The outer domain was designed to simulate the large-scale atmospheric environment, including the typhoon structure, whereas the inner domain was designed to use the input for the storm surge simulations. The initial and lateral boundary conditions for the WRF-Jebi were derived from the Japanese 55-year Reanalysis Project datasets (JRA55; Kobayashi et al., 2015; details are available online at http://jra.kishou.go.jp/JRA-55/index_en.html). Only the outer domain was initialized and forced by JRA55, which were modulated using the T-TES method and used as the initial and boundary atmosphere data. The inner domain was initialized and forced based on the outer domain results every 45-90 seconds through 24 h integration as the initial and boundary atmosphere data. Details of the inner-domain initial atmosphere data are provided in Appendix A. The integration period for the outer domain was from 0000 UTC on 2 September to 0000 UTC on 5 September, 2018, while for the inner domain was from 0000 UTC on 3 September to 0000 UTC on 5 September, 2018. Table 1 summarizes the WRF settings.

Table 1

A parametric TC model (Para-Jebi) was also used to estimate the surface winds and sea-level pressure distributions associated with 83 tracks of Typhoon Jebi with the same tracks and intensities as WRF-Jebi. The axisymmetric sea-level pressure was derived using the formula proposed by Fujita (1952), and the surface wind distribution was calculated from the gradient wind equation. The effect of typhoon movement was determined using the equation proposed by Miyazaki (1961). The surface friction coefficient, which represents the ratio of surface wind to gradient wind, was set to 0.7 in this study. This value was empirically determined based on observed winds and various simulation results. Details about the parametric TC model can be found in previous papers (e.g., Meteorological Research

Institute of Japan Meteorological Agency (JMA), 2000, Kohno et al.,2001, 2007, Hossain et al, 2017). To allow comparison with the meteorological model, the other computational settings conditions for the Para-Jebi were the same in all simulations; i.e., the typhoon position, central pressure, the maximum wind, and radius of maximum wind used in the Para-Jebi were determined by the results of the WRF-Jebi obtained at 3-h intervals. It is complemented by linear interpolation between the inputs.

In this study, the storm surge simulations were conducted using a storm surge model developed by the JMA. Table 2 summarizes the calculation parameters used in the storm surge model. This model has been used in previous research such as Kohno et al. (2007), Kuroda et al. (2010), Hossain et al. (2017), and Kohno et al. (2018). The bathymetric conditions used in the model were based on the ETOPO1 bathymetry data (National Oceanic and Atmospheric Administration: https://ngdc.noaa.gov/mgg/global/). Simulations were conducted using a horizontal resolution of 1.7 km. The 1.7-km grid resolution was used in previous operations of JMA (JMA, 2007) and case studies (e.g., Kohno et al., 2007), and it gave reasonable results. The sea surface stresses are estimated with a constant drag coefficient ($Cd=3.2\times10^{-3}$) which is a typical value in stormy winds. Additionally, typical storm surge mechanisms for the inverse barometer effect and wind setup were considered. Astronomical tides and wave effects were not considered because the focus was to evaluate possible storm surges.

Table 2

3. Results

3.1 Storm surge simulation at Osaka Port

This study compared the maximum storm surges at Osaka Port derived by observations and both models. Figure 1 shows the track of Typhoon Jebi simulated in the inner domain, Fig.1 with elevation above sea level around the Kinki district. The positions of WRF-Jebi were determined from the area of minimum sea-level pressure. The track, which was shifted eastward by 0.4° at the initial time using T-TES, was closest to the actual track of Typhoon Jebi from the best track archives (BT) of the Regional Specialized Meteorological Centers–Tokyo Typhoon Center, around the Shikoku and Kinki districts. This simulation was defined as the control run (CTL), in which WRF-Jebi made landfall at Osaka Port around 0520 UTC on 4 September, 2018, 20 min after the actual time.

Time series of the central pressure and radius of maximum winds of Typhoon Jebi, derived from the BT and CTL of WRF-Jebi, are shown in Figure 2 and Table 3. In the BT, Fig.2 Table 3 Typhoon Jebi had a central pressure of 960 hPa when it was closest to Osaka Port at 0500 UTC on 4 September, 2018. The central pressure of WRF-Jebi differed from that derived from BT by the end of 3 September and this discrepancy was not clear. However, the central pressure simulated at 0530 UTC 4 September 2018 was about 966 hPa, which fairly compared with that of the BT. The track and intensity of Typhoon Jebi around the Shikoku and Kinki districts were well reproduced by the WRF-Jebi.

Fig.3

Figure 3 shows a time series of the storm surge observed at Osaka Port, and that estimated by the storm surge model with both input models. The maximum storm surge of 2.73 m was observed at Osaka Port. The maximum storm surge of 2.49 m estimated using the WRF-Jebi inputs was slightly lower than the observation (difference of 0.24 m). The maximum storm surge estimated using the WRF-Jebi inputs occurred 20 min later than the observation. The maximum storm surge estimated using the Para-Jebi inputs (2.11 m) was lower than the observation by 0.62 m.

Fig.4

There were differences in the storm surges estimated using the WRF-Jebi and Para-Jebi inputs. This discrepancy was not attributed to the inverse barometer effects, but rather to the wind setup effect. The storm surge caused by the inverse barometer effect for WRF-Jebi was 0.46 m, while for Para-Jebi it was 0.42 m. The wind setup effect for WRF-Jebi was about 2.03 m, which was larger than that for Para-Jebi (1.69 m). Figure 4 shows the surface winds around the Kinki district at 0500 UTC and 0520 UTC on 4 September. According to a JMA mesoscale analysis (MSM), a strong local wind area exceeding 35 $m \cdot s^{-1}$ was estimated over Osaka Bay. The WRF-Jebi reproduced a similar local wind area, of approximately 30 $m \cdot s^{-1}$, which agreed well with the MSM. According to data from the Behavior of Hypoxia in Osaka Bay project (http://teiten.pa.kkr.mlit.go.jp/obweb/data/c1/c1_12.aspx), the maximum wind speed at Osaka Bay in Typhoon Jebi at 0600 UTC on 4 September 2018 was 28.7

m·s^{-1}, which agreed well with the WRF-Jebi. On the other hand, in the Para-Jebi the surface wind was below 25 m·s^{-1} over Osaka Bay and there was no strong local wind. Unlike the WRF-Jebi, the Para-Jebi was not influenced by topography, and was therefore unlikely to produce realistic winds in areas with a complex topography.

3.2 Ensemble experiments at Osaka Port

Our ensemble experiments using the T-TES method estimated storm surges and longitudinally perturbed “worst-case course” assuming various tracks for Typhoon Jebi at Osaka Port. Figure 5 shows the 83 typhoon tracks according to different central pressure Fig.5 and radius of maximum wind values, obtained from ensemble experiments using the T-TES method. The tracks were almost parallel to each other. The central pressure of Typhoon Jebi varied among the courses, with the values tending to be the same before making landfall on the Japanese Islands and increasing thereafter. The temporal changes in the radius of maximum wind remained small over the ocean and increased after making landfall on the Japanese Islands.

The maximum storm surges at Osaka Port are shown in Figure 6a for different typhoon Fig.6 tracks using the T-TES method. When Typhoon Jebi passed east of Osaka Port, the maximum storm surge was low; however, it was higher when it passed west of Osaka Port. The “hit course” was 0.2° to the east relative to the CTL, and the maximum storm surges were 2.00 m and 2.11 m in the simulations using the WRF-Jebi and Para-Jebi inputs, respectively. Here, "hit course" stands for the course where the center of a typhoon crosses just over the target location (here, Osaka Port) and is shown as 0.0º in Fig. 6. For all tracks, the CTL had a maximum storm surge of 2.49 m when estimated using the WRF-Jebi input, which represented the worst-case longitudinally perturbed course of Typhoon Jebi for the storm surge at Osaka Port. In contrast, the estimate using the Para-Jebi input had a higher storm surge of 2.30 m when the typhoon track was 0.4° west of the hit course.

In Fig. 6a, the maximum storm surge calculated using the Para-Jebi smoothly changed, which gradually increased as tracks approached to the worst-course from west and decreased as tracks moved away from the worst course. In contrast, the estimates using the WRF-Jebi inputs abruptly increased as tracks shifted from 0.8° west of the CTL to 0.6° west. Figure 7 shows the surface winds around the Kinki district at the time of the maximum Fig.7 storm surges in cases of 0.6° and 0.8° west of the hit course. Although there was little difference in the wind speeds over Osaka Bay between the two tracks, the wind direction over Osaka Bay changed from south-southwesterly in the 0.6° west course to southerly in the 0.8° west course. The topography around Osaka Bay was responsible for the changes in direction of the surface wind over Osaka Bay. Osaka Bay is surrounded by mountains with a relatively high altitude rather than flat lowlands (Fig. 1b).

Figure 6a also shows the occurrence time of the maximum storm surge in both models, which was determined by the time elapsed from the time of minimum sea-level pressure at each location (here, Osaka Port) for each track. Note that a negative (positive) time means before (after) the time of the minimum sea level pressure, i.e., Typhoon Jebi was approaching (leaving). In both models, the occurrence time of the maximum storm surges were about 60 min in the worst-case courses. The difference in occurrence time between both models increased with the distance between the hit course and Osaka Port.

3.3 Assessment of the worst-case storm surge along the coastal region

Ensemble experiments estimated storm surges and longitudinally perturbed “worst-case courses” assuming various tracks for Typhoon Jebi in other coastal areas. Figure 6b shows the maximum storm surges and their occurrence times at Nagoya Port. The distribution of the maximum storm surges at Nagoya Port was similar to that at Osaka Port. The maximum storm surge estimated using WRF-Jebi inputs was 2.83 m in case of 0.4° west of the hit course, which was much larger than that estimated using the Para-Jebi inputs (1.87 m). Figure 8 shows the surface winds around Ise Bay at 0530 UTC on 4 September when the maximum storm surge occurs, derived by both models in case of 0.4º west of the hit course for Nagoya Port. The large differences in the maximum storm surge between both models was due to the wind setup effect. Fig.8

Figures 6c and 6d show the maximum storm surges and their occurrence times at

Unoshima Port and Kushimoto Port, respectively. Unoshima Port is located in Suo Nada and faces north, toward the ocean (Fig. 1a). The maximum storm surges were lower when Typhoon Jebi passed west of Unoshima Port but became higher when Typhoon Jebi passed east of the port. At Kushimoto Port, the maximum storm surges from all ensemble experiments were less than 1.00 m. Because Kushimoto Port faces the deep ocean and has a depth greater than 100 m (not shown), the wind setup effect is not crucial. None that the typhoon tracks caused a large storm surge at Kushimoto Port. However, wave setup can be a key factor in storm surges on coasts such as Kushimoto Port, when high waves hit (e.g., Kohno et al., 2018, Washida et. al., 2019). Because wave setup is a local phenomenon that only exerts a crucial effect in specific areas, as revealed by other studies of storm surges, its effects were not considered here. However, its effects are important when assessing the overall risk to the coast, especially including areas which face to open ocean, so it will be the subject of future research.

Figure 9 shows maps of the maximum storm surges along the coastline of the main Fig.9 island, Shikoku, and Kyushu. According to simulations using the inputs from both models, maximum storm surges over 2.50 m could occur in the Ariake Sea, Suo Nada, Hiroshima Bay, Osaka Bay, Ise Bay, Mikawa Bay, Tokyo Bay, and Sendai Bay. The regions most at risk were open shallow bays less than 50 m in depth (not shown). At coastal areas of Seto Inland Sea, maximum storm surges over 2.50 m occurred at some locations in Suo Nada and

Hiroshima Bay, and surges over 1.50 m occurred at locations between Yamaguchi and Okayama Prefectures. Specifically, the maximum storm surge occurred in the innermost point of the bay. The largest maximum storm surge in Japan based on WRF-Jebi was 3.22 m in the coastal area of Osaka Bay, whereas that based on Para-Jebi was 2.94 m at Togari Port in the Ariake Sea.

Figure 10 shows the maximum storm surges and worst-case courses in the coastal region from Izumo to Choshi (Fig. 1a), according to simulations using both models input. There were 1,896 sampling points in this coastal region. The maximum storm surges at most points estimated using WRF-Jebi inputs were generally larger than those estimated using Para-Jebi inputs. The average difference in maximum storm surges between both models was 0.37 m. The maximum difference of 1.19 m occurred at Nagoya Port near Point C (Fig. 1a). The difference between both models increased at points with larger maximum storm surges. In most coastal region, the models predicted almost the same worst-case course. At coastal ports facing north, such as the Unoshima Port near Point I (Fig. 1a and Fig. 6a), the worst-case course was on the eastern side of the hit course. The differences in storm surges associated with the west–east courses of TCs depended on the ocean-facing direction of the bay. Fig.10

This study conducted ensemble experiments to estimate areas at risk of a large storm surge. Table 4 shows the relative proportions of maximum storm surges and worst-case Table 4 courses in each coastal region as shown in Fig. 1c. Note that 6,285 coastal points were considered at equal space intervals. Coastal areas where the maximum storm surge was produced by a track within 0.2° of the hit courses were defined as hit course areas. Coastal areas where the worst-case course was at least 0.4° east (west) of the hit course were defined as east (west) course areas. The percentage in Table 4 is defined by the ratio of the coastal points where the maximum storm surge exceeds 1.00m/2.00m to the number of coastal points in each coastal area.

For the main island, Kyushu, and Shikoku, 5.9% of the maximum storm surges were more than 2.00 m in extent, while 26.8% were in the range of 1.00–2.00 m. The proportion of maximum storm surges occurring on the main island was almost the same as the average for all areas. Although the maximum storm surge in Shikoku never exceeded 2.00 m, 45.8% of the maximum storm surges were in the range of 1.00–2.00 m, which was larger than the values for the main island and Kyushu. In Kyushu, 7.0% of the maximum storm surges were more than 2.00 m in extent, which was the largest proportion among all areas studied. About 55% of the worst-case courses in the main island followed the hit course area, and about 35% (10%) followed the west (east) course area. In Shikoku, about 50% of all worst-case courses followed the hit course area and the west course area, and there were no cases following the east course area. In Kyushu, about 65% of all worst-case courses followed the hit course area and about 30% (5%) followed the west (east) course area.

At R1 and R2 on the main island, only 4.7% of the maximum storm surges were more than 1.00 m in extent, indicating that high storm surges are rare. Notably, maximum storm surges of more than 1.00 m in extent at R6 on the main island were seen in 100% of cases. The coastline at R6 is at high risk of storm surges, in part due to the presence of an open shallow bay. In Shikoku, there was a large difference between the north side (R7) and south side (R8). At R8, 10.5% of the maximum storm surges were more than 1.00 m in extent, compared to 73.9% at R7. In this study, Kyushu was divided into the west side (R9) and east side (R10). At R9, 51.1% of maximum storm surges were more than 1.00 m, compared to 35.7% at R10. Storm surges in Kyushu were more dangerous in the west coast than in the east coast. From the entire results, the largest maximum storm surge was in Osaka Bay, which is the R4 region. Osaka Bay would be attributed not only the open shallow bay but also the track of Typhoon Jebi. Since direction of Typhoon Jebi movement around the Japanese Island is north-northeast and Osaka Bay opened to the southwest in almost parallel to the movement direction, the maximum storm surge became the largest. The values of the maximum storm surges estimated by T-TES for Typhoon Jebi may be slightly different from those for other typhoons, which will research other typhoon cases in the future; the results should provide useful information for disaster risk management.

4. Discussion and summary

This study estimated the maximum storm surges caused by Typhoon Jebi using the JMA storm surge model in conjunction with simulations based on the meteorological (WRF-Jebi) and parametric TC (Para-Jebi) models. The maximum storm surge at Osaka Port estimated using WRF-Jebi inputs (2.49m) was closer to the observed storm surge (2.73m) than that estimated using Para-Jebi inputs (2.11m). We found that the difference between both models was caused by the wind setup effect rather than the inverse barometer effect. In the Typhoon Jebi case, the average difference in maximum storm surges between both models was 0.37 m, and the maximum of difference of 1.19 m was found at Nagoya Port near Point C (Fig. 1a). The topography effect might have enhanced the surface winds over Osaka Bay; the parametric TC model could not account for this effect, whereas the meteorological model could, leading to an increase in storm surges due to the wind setup effect according to WRF-Jebi.

Our ensemble experiments based on the T-TES method indicated that the maximum storm surge varied with longitudinal perturbation of the track of Typhoon Jebi along the entire coast of the Japanese Islands, including the main island, Kyushu, and Shikoku. The difference between both models increased at locations where the maximum storm surge was larger. The worst-case courses for each coastal area were almost the same track for both models.

Our ensemble experiments showed that during the passage of Typhoon Jebi, maximum storm surges of over 2.50 m occurred in coastal areas in the Ariake Sea, Suo Nada, Hiroshima Bay, Osaka Bay, Ise Bay, Mikawa Bay, Tokyo Bay, and Sendai Bay. These regions were typically shallow bays that were less than 50 m deep. In almost all coastal areas with large maximum storm surges, the worst-case course occurred 0.4–0.8° west of the hit course because the wind setup exerted an important effect on the larger maximum storm surges. The distance between the worse-case and hit courses was consistent with the radius of maximum wind of Typhoon Jebi.

This study estimated the coastal regions where large storm surge are possible. For the main island, Kyushu, and Shikoku, 5.9% of the maximum storm surges were more than 2.00 m in extent, while 26.8% were in the range of 1.00–2.00 m. For coasts of the main island facing the Japanese sea, 1.5% of the maximum storm surges were more than 1.00 m in extent; high storm surges were therefore rare. In coastal areas of Seto Inland Sea, there was a large risk of high storm surges due to the presence of an open shallow bay. Storm surges in Shikoku (Kyushu) were more dangerous on the north (west) than south (east) coast.

The exact reasons how the surrounding topography enhances/suppress the surface winds over the Osaka Bay and Ise Bay remain unclear. Further, this study was based only on Typhoon Jebi; whether the results generalize to other typhoons are needed. However, our simulations pertained to storm surges and worst-case courses for almost the entire coastline of Japan. Because our simulations cover all areas including where no significant storm surge by a typhoon is recorded, the results will be surely useful information for disaster risk management, they provide important information for disaster risk management.

Acknowledgments

The authors thank Drs. M. Toyoda, K. Tsuji, S. Yamasaki, and Y. Kiyohara for their support with the data analysis. This work was supported by the Collaborative Research Project on Computer Science with High-Performance Computing at Nagoya University (2018) and the Integrated Research Program for Advancing Climate Models (TOUGOU program) from the Ministry of Education, Culture, Sports, Science and Technology (MEXT) of Japan. This work was also supported by the MEXT KAKENHI (Grant Nos. 17K14398, 19H05696, and 21K03658).

Appendix A:

The typhoon track ensemble simulation (T-TES) method, which was developed by a Yamasaki et al. (2017), was used in this research. Only the outer domain of the meteorological model used atmospheric data derived from JRA55, which was modulated using the T-TES method to derive the initial and boundary atmosphere data. The inner domain used the atmospheric data from outer-domain simulation results, with a 24 h integration, as the initial and boundary atmosphere data. Figure A1 shows the initial atmosphere data of the inner domain, such as surface winds and sea-level pressure, for the CTL, 3.0° west, and 3.0° east simulations. It can be seen that the locations of the typhoons were shifted eastward or westward from that of the CTL. The surface wind and sea-level pressure differed among the ensemble simulations. The wind direction over the Japanese Islands changes due to the topography of the area. Therefore, the surface winds were simulated considering both the large-scale atmospheric field and topographic effects.

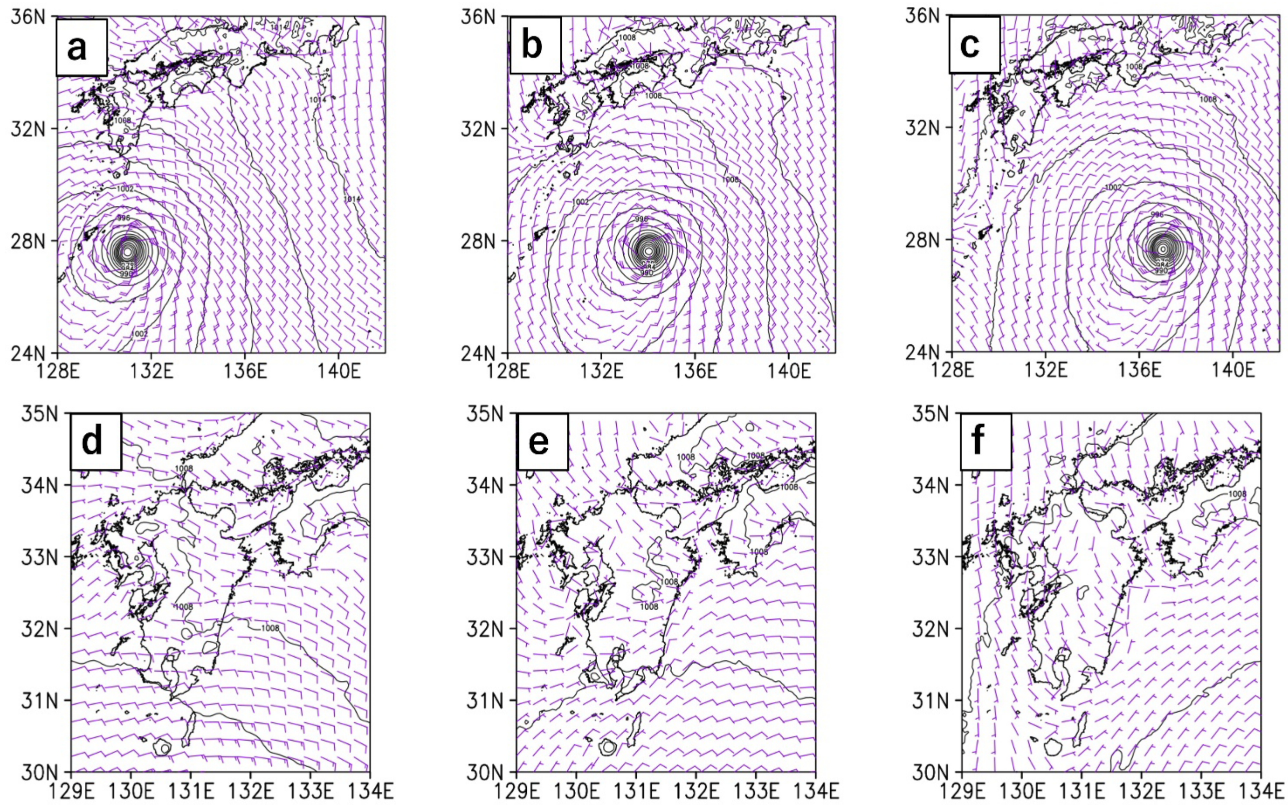

Figure A1: Surface winds (wind barbs) and sea-level pressure (contours) simulated in the inner domains at the initial time of 0000 UTC on 3 September (a) (d) 3.0°west of the CTL, (b) (e) at the CTL, and (c) (f) 3.0°east of the CTL. A full wind barb represents 50 m·s^{-1} and a contour interval is 3 hPa.

References

Colle, A., J. Bowman, J. Roberts, M. Bowman, N. Flagg, J. Kuang, Y. Weng, B. Munsell, and F. Zhang, 2015: Exploring water level sensitivity for metropolitan New York during Sandy (2012) using ensemble storm surge simulations, *J. Mar. Sci. Eng*. **3** 428-443, doi:10.3390/jmse3020428.

Fujita, T., 1952: Pressure distribution within typhoon, *Geophysical Magazine*, **23**, 437-451.

Gao, Y., H. Wang, G. M. Liu, X. Y. Sun, X.Y. Fei, P.T. Wang, T. T. Lv, Z. S. Xue, and Y. W. He, 2013: Risk assessment of tropical storm surge for coastal regions of China, *J. Geophys. Res. Atmos.*, **119**, 5354-5374, doi:10.1002/2013JD021268.

Hossain, MA., SMQ. Hassan, MB. Rashid, MAK. Mallik, MS. Islam, 2017: Storm surge simulation of Cyclone "Roanu" over coastal regions of Bangladesh using MRI storm surge model, *DEW-DROP*, **3**, 46-54.

JMA, 2000: Report on the Storm Surges by Typhoon Bart (No.9918) in September 1999, Japan, *Technical report of the Japan Meteorological Agency*, **122**, 15-38 (in Japanese).

JMA, 2018: Wind storm and storm surges by Typhoon No. 21. 2018 (In Japanese). [Available at : http://www.data.jma.go.jp/obd/stats/data/bosai/report/2018/20180911/jyun_sokuji20180903-0905.pdf.]

Kobayashi, S., Y. Ota, Y. Harada, A. Ebita, M. Moriya, H. Onoda, K. Onogi, H. Kamahori, C. Kobayashi, H. Endo, K. Miyaoka, and K. Takahashi, 2015: The JRA55 reanalysis: general specifications and basic characteristics, *J. Meteor. Soc. Japan*, **93,** 5-48, doi:10.2151/jmsj:2015-001.

Kohno, N., 2001: The storm surges in the Sea of Yatsushiro generated TY9918 (BRAT). *Umi to Sora* (Sea and Sky), **76**, 207-213 (in Japanese).

Kohno, N., K. Kamakura, H. Minematsu, Y. Yorioka, K. Hisashige, E. Shimizu, Y. Sato, A. Fukunaga, Y. Taniwaki, and S. Tanijyo, 2007: The Mechanism of the Storm Surges in the Seto Inland Sea Caused by Typhoon Chaba (0416), *RSMC Tokyo – Typhoon Center, Technical Review*, **9**, 1-18.

Kohno, N., S. K. Dube, M. Entel, S.H.M. Fakhruddin, D. Greenslade, M. D. Leroux, J. Rhome, and N. B. Thuy, 2018: Recent progress in storm surge forecasting, *Tropical Cyclone Research and Review*, **7,** 128-139.

Kowaleski, M., E. Morss, D. Ahijevych, R. Fossell, 2020: Using a WRF-ADCIRC ensemble and track clustering storm surge hazards and inundation scenarios associated with Hurricane Irma, *Weather and Forecasting,* **35**, 1289-1315.

Kuroda, T., K. Saito, M. Kunii, and N. Kohno, 2010: Numerical simulations of Myanmar Cyclone Nargis and the associated storm surge Part I: Forecast experiment with a nonhydrostatic model and simulation of storm surge, *J. Meteor. Soc. Japan.* **88,** 521-545.

Miyazaki, M., T. Ueno, and S. Unoki, 1961: Theoretical investigations of typhoon surges along the Japanese coast, *Oceanographical Magazine*., **13**, 51-75.

MLIT, 2021; Storm surge inundation area map creation guide Ver 2.10, pp90 (in Japanese). [Available at https://www.mlit.go.jp/river/shishin_guideline/kaigan/takashioshinsui_manual.pdf.]

Mori, N., T. Yasuda, T. Arikawa, T. Kataoka, S. Nakajo, K. Suzuki, Y. Yamanaka, A. Webb, 2019a: 2018 Typhoon Jebi post-event survey of coastal damage in the Kansai region, Japan, *Coastal Engineering Journal*, **61**, 278-294.

Mori, N., T. Shimura, K. Yoshida, R. Mizuta, Y. Okada, M. Fujita, T. Temur Khujanazarov, E. Nakakita, 2019b: Future changes in extreme storm surges based on mega-ensemble projection using 60-km resolution atmospheric global circulation model, *Coastal Engineering Journal,* **61**, pp.295-307.

Mori, N., N. Fukui, and T. Shimura, 2020: A review of maximum storm surge heights in Japanese three major bays considering climate change, *J. Soc. Civ. Engineering*. *B2*, **76**, 1-6 (in Japanese).

Mori, N., N. Ariyoshi, T. Shimura, T. Miyashita, J. Ninomiya, 2021: Future projection of maximum potential storm surge height at three major bays in Japan using the maximum potential intensity of a tropical cyclone, *Climatic Change,* **164**, 3-4.

Nakajo, S., N. Mori, T. Yasuda and H. Mase, 2014: Global stochastic tropical cyclone model based on principal component analysis and cluster analysis, *Journal of Applied Meteorology and Climatology,* **53**, 1547-1577.

Ninomiya, J., N. Mori, T. Takemi and O. Arakawa, 2017: SST ensemble experiment-based impact assessment of climate change on storm surge caused by pseudo-global warming - Case study of Typhoon Vera in 1959, *Coastal Engineering Journal*, **59**, 1-20.

JMA, 2007: Outline of the operational numerical weather prediction at the Japan Meteorological Agency. [Available at https://www.jma.go.jp/jma/jma-eng/jma-center/nwp/outline2007-nwp/index.htm.]

Shibutani, Y., S. Nakajo, N. Mori, S. Kim, and H. Mase, 2015: Estimation of worst-class tropical cyclone and storm surge, and its return period -case study for Ise Bay-. *J. Soc. Civ. Engineering. B2*, **71**, 1513-1518 (in Japanese).

Skamarock, W. C., J. B. Klemp, J. Dudhia, D. O. Gill, D. M. Barker, M.G. Dura, X. Huang, W. Wang, and J. G. Powers, 2008: A description of the advanced research WRF version 3, NCAR, Tech. Note, Mesoscale and Microscale Meteorology Division, *National Center for Atmospheric Research*, Boulder, Colorado, USA.

Takabatake, T., M. Mäll, M. Esteban, R. Nakamura, T. O. Kyaw, H. Ishii, J. J. Valdez, Y. Nishida, F. Noya, and T. Shibayama, 2018: Field Survey of 2018 Typhoon Jebi in Japan: *Lessons for disaster risk management, Geosciences*, **8**, 412-431.

Takemi, T., T. Yoshida, S. Yamasaki, and K. Hase, 2019: Quantitative estimation of strong winds in an urban district during Typhoon Jebi (2018) by merging mesoscale meteorological and large-eddy simulations. *SOLA*, **15**, 22-27, doi:10.2151/sola.2019-005.

Thuy, N.B., H. D. Cuong, D. D. Tien, D. D. Chien, and S. Y. Kim, 2014: Assessment of changes in sea-level caused by Typhoon Kalmaegi Sept./2014 and forecast problems. *Scie. and Tech. Hydro-Met. J*, **647**, 16-20.

Toyoda, M., J. Yoshino, M. Hayashi, and T. Kobayashi, 2020: Dynamic evaluations of the worst storm surge in Tokyo Bay and Ise Bay induced by typhoon Hagibis (2019), *J. Soc. Civ. Engineering. B2*, **76**, 133-138 (in Japanese).

Washida, M., N. Muroi, and T. Takahashi,2019; Numerical analysis of typhoon-induced wave setup surges along west coast of Sagami Bay, *Japan Society of Civil Engineers*, **75,** 61-66 (in Japanese).

Yamasaki, S., H. Fudeyasu, M. Kato, T. Takemi, and Y. Kiyohara, 2017: Assessing typhoon wind hazerd: Development of typhoon nomogram, *J. of wind Engineering*, **42**, 121-133 (in Japanese).

Yang, J.A, S.Y. Kim, S.Y. Son, N. Mori, H. Mase, 2020: Assessment of uncertainties in projecting future changes to extreme storm surge height depending of future SST and greenhouse gas emission scenarios, *Climatic Change*, **162**, 425-442.

Yasuda, T., S. Nakajo, S. Kim, H. Mase, N. Mori and K. Horsburgh, 2014: Evaluation of future storm surge risk in East Asia based on state-of-the-art climate change projection, *Coastal Engineering Journal,* **83**, 65-71.

List of figure and table

meteorological simulation (purple, right axis).

Figure 3: Time series of the storm surges at Osaka Port derived from observations (red) and JMA storm surge model. Typhoon Jebi was simulated using the meteorological (green) and parametric TC (blue) models.

Figure 4: Surface winds at 10 m height (wind barbs, a full wind barb represents 50 $m \cdot s^{-1}$), wind speeds, and sea-level pressure (contour, contour interval is 3 hPa) derived from (a) the meteorological model (CTL), (b) the parametric TC model (CTL) at 0520 UCT on 4 September, and (c) the MSM at 0500 UCT on 4 September. The maximum wind radius for Para-Jebi is based on the results of WRF-Jebi. (d) The difference between WRF-Jebi to Para-Jebi wind speed at 0520 UTC on 4 September. Time series of surface winds derived from (e) the meteorological model (CTL), (f) the parametric TC model (CTL), and (g) MSM at Osaka Port. One full wind barb is 50 $m \cdot s^{-1}$. The typhoon positions, central pressure, and radius of maximum wind used in Para-Jebi were based on the results of WRF-Jebi.

Figure 5: Tracks of Typhoon Jebi simulated by WRF ensemble experiments using the (a) central pressure and (b) radius of maximum wind of Typhoon Jebi.

Figure. 6: Maximum storm surge (bar) and occurrence time (line) for various tracks of Typhoon Jebi relative to the hit course at (a) Osaka Port, (b) Nagoya Port, (c) Unoshima Port, and (d) Kushimoto Port. Plots were derived from the JMA storm surge model, with

Typhoon Jebi simulated by the meteorological (green) and parametric TC (blue) models. The red triangle indicates the CTL, which is 3.4° to the east of the hit course for Unoshima Port. The observed maximum storm surges are shown in the graph, excluding Unoshima.

Figure 7: Surface winds at 10 m height (wind barbs, a full wind barb represents $m \cdot s^{-1}$.), wind speeds (shaded), and sea-level pressure (contour, contour interval is 3 hPa) simulated by (a) (b) the meteorological model and (c) (d) the parametric TC model at 0530 UTC on 4 September 2018, at (a) (c) 0.8° and (b) (d) 0.6° west of the hit course for Osaka Port.

Figure 8: Surface winds at 10 m height (wind barbs, a full wind barb represents 50 $m \cdot s^{-1}$.), wind speeds (shaded), and sea-level pressure (contour, contour interval is 3 hPa) simulated in (a) the meteorological model and (b) the parametric TC model at 0530 UTC on 4 September (the timing of the maximum storm surge), 0.4° west of the hit course for Nagoya Port. (c) The difference between WRF-Jebi to Para-Jebi surface wind at 0530 UTC on 4 September.

Figure 9: Maps of the maximum storm surges derived from the JMA storm surge model, with Typhoon Jebi simulated by (a) the meteorological model and (b) the parametric TC model.

Figure 10: (a) Maximum storm surges and (b) the worst-case courses in coastal areas from Izumo to Choshi. Lines are derived from the JMA storm surge model, with Typhoon Jebi simulated by the meteorological (green) and parametric TC (blue) models.

Table 1: Conditions used in the WRF model.

	Outer domain	Inner domain
Horizontal resolution (km)	15	5
Horizontal grid	220 × 215	601 × 541
Calculation period	2018/9/2/0000UTC– 2018/9/5/0000UTC	2018/9/3/0000UTC– 2018/9/5/0000UTC
Ground data	GTOPO30	
Vertical layers	45	
Bottom altitude (m)	~30	
Top altitude (hPa)	20	
Microphysics scheme	WSM 6-class graupel scheme	
Radiation scheme	Rapid Radiative Transfer Model For GCM	
Atmospheric boundary layer scheme	Yonsei University scheme	
Convection scheme	Kain-Fritsch scheme	
Typhoon bogus scheme	Include	None
Shift interval	0.2°	
Output interval	30 min	
Initial value / boundary condition	JRA55	

Table 2: Conditions of the JMA storm surge model.

Horizontal resolution (km)	1.7
Horizontal grids	811 × 361
Output interval (min)	10
Initial condition	Static state
Outer boundary	Balanced to slp
Land boundary	Wall (wet / dry)
Bathymetry data	ETOPO1
Astronomical tides	Not included
Meteorological input	Parametric / GPVs
Calculation area (north)	N 36.0–42.0°
	E 133.0–146.5°
Calculation area (south)	N 30.0–36.0°
	E 128.0–141.5°

Table 3: Time series central pressure of BT and WRF-Jebi.

number	Time	Best track(red)	WRF-Jebi(green)
1	0000UTC 3 Sep.	940 hPa	959 hPa
2	0012UTC 3 Sep.	940 hPa	959 hPa
3	0000UTC 4 Sep.	950 hPa	956 hPa
4	0012UTC 4 Sep.	970 hPa	975 hPa
5	0000UTC 5 Sep.	-	983 hPa

Table 4: The maximum storm surge for each coastal region in Typhoon Jebi divided into less than 1 m, 1–2 m, and more than 2 m, and the worst-case course divided into west, hit, and east courses. The table shows the percentages and number of points in each region.

Region	Total	Maximum storm surge (m)			Worst-case course		
		-1.00	1.00-2.00	2.00-	West course	Hit course	East course
All	6285	67.4%(4235)	26.8%(1682)	5.9%(368)	34.7%(2181)	57.3%(3602)	8.0%(502)
Main Island	4138	74.1%(3068)	19.4%(803)	6.5%(267)	33.4%(1381)	55.5%(2296)	11.1%(461)
Shikoku	710	54.2%(385)	45.8%(325)	0.0%(0)	52.0%(369)	48.0%(341)	0.0%(0)
Kyushu	1437	54.4%(782)	38.6%(554)	7.0%(101)	28.9%(415)	66.9%(961)	4.2%(61)
R1	1722	98.5%(1697)	1.5%(25)	0.0%(0)	25.2%(434)	61.0%(1050)	13.8%(238)
R2	606	86.0%(521)	12.5%(76)	1.5%(9)	27.4%(166)	62.0%(376)	10.6%(64)
R3	439	61.0%(268)	31.7%(139)	7.3%(32)	27.3%(120)	72.0%(316)	0.7%(3)
R4	631	69.7%(440)	23.6%(149)	6.7%(42)	23.6%(149)	74.6%(471)	1.7%(11)
R5	298	47.7%(142)	35.6%(106)	16.8%(50)	47.3%(141)	49.3%(147)	3.4%(10)
R6	442	0.0%(0)	69.7%(308)	30.3%(134)	83.9%(371)	12.7%(56)	3.4%(15)
R7	395	26.1%(103)	73.9%(292)	0.0%(0)	81.3%(321)	18.7%(74)	0.0%(0)
R8	315	89.5%(282)	10.5%(33)	0.0%(0)	15.2%(48)	84.8%(267)	0.0%(0)
R9	917	48.9%(448)	41.2%(378)	9.9%(91)	38.1%(349)	59.4%(545)	2.5%(23)
R10	520	64.2%(334)	33.8%(176)	1.9%(10)	15.8%(82)	80.8%(420)	3.5%(18)

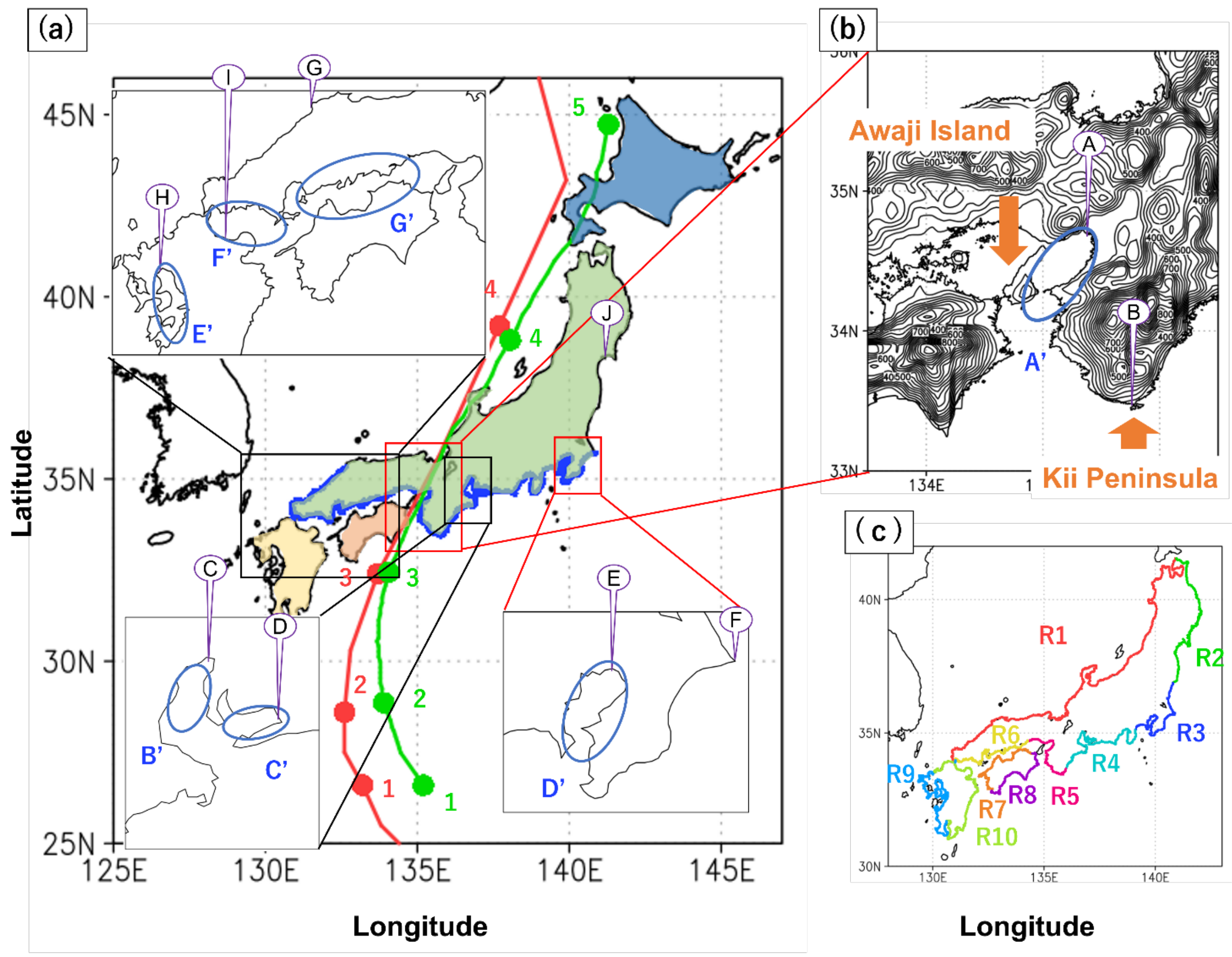

Figure 1: (a) Tracks of Typhoon Jebi derived from the WRF simulation in the CTL (green) and best track (red). Dots along the track indicate the location of Typhoon Jebi, measured at 12-h intervals, and the central pressure at that time is summarized in Table 3. The blue line indicates the coastal region (see Fig. 10). (b) Elevation above sea level around the Kinki district. Contour interval is 50 m. (c) Coastal regions (see Table 4). Blue area: Hokkaido, green area: Main Island, orange area: Shikoku, Yellow area: Kyushu. Point A: Osaka Port, B: Kushimoto port, C: Nagoya Port, D: Mikawa Port, E: Tokyo, F: Choshi Port, G: Izumo, H: Togari Port, I: Unoshima Port, and J: Sendai. Area A': Osaka Bay, B': Ise Bay, C': Mikawa Bay, D': Tokyo Bay, E': Ariake Sea, F' Suo Nada, and G'; Set Island Sea.

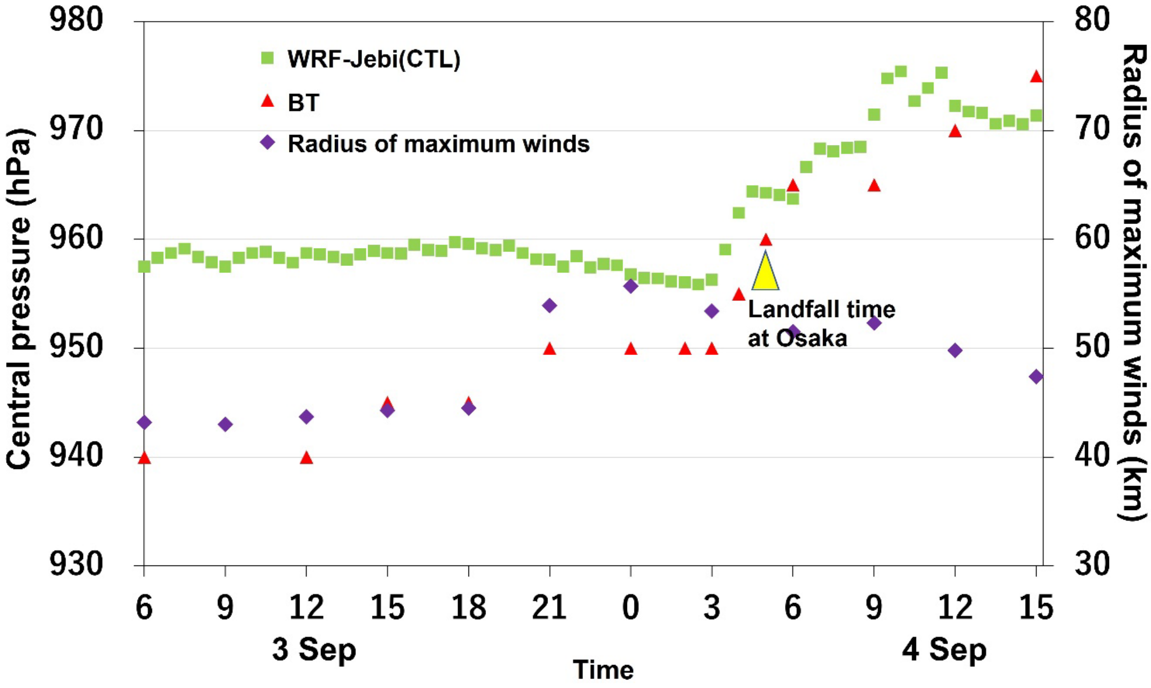

Figure 2: Time series of the central pressure of Typhoon Jebi derived from a meteorological simulation (green), the best track (red), and the radius of maximum wind according to a meteorological simulation (purple, right axis).

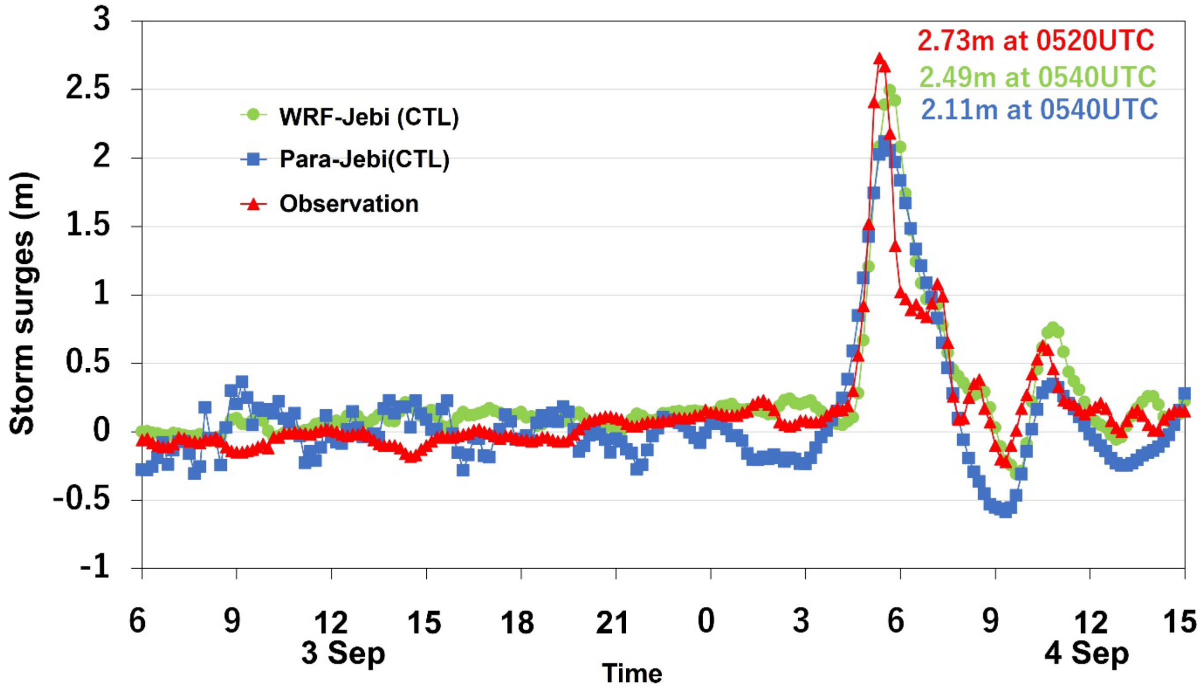

Figure 3: Time series of the storm surges at Osaka Port derived from observations (red) and JMA storm surge model. Typhoon Jebi was simulated using the meteorological (green) and parametric TC (blue) models.

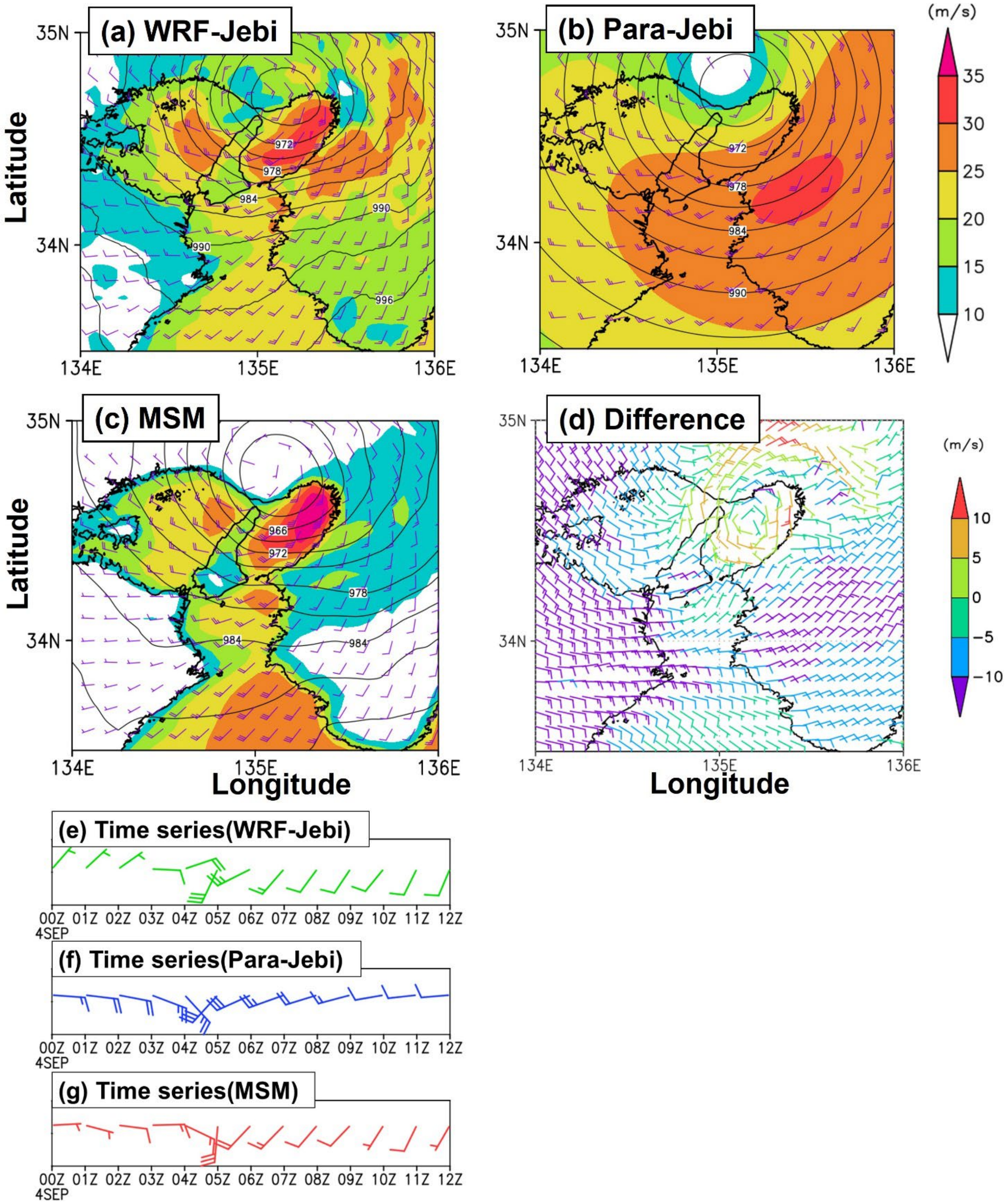

Figure 4: Surface winds at 10 m height (wind barbs, a full wind barb represents 50 m·s^{-1}), wind speeds, and sea-level pressure (contour, contour interval is 3 hPa) derived from (a) the meteorological model (CTL), (b) the parametric TC model (CTL) at 0520 UTC on 4

September, and (c) the MSM at 0500 UCT on 4 September. The maximum wind radius for Para-Jebi is based on the results of WRF-Jebi. (d) The difference between WRF-Jebi to Para-Jebi wind speed at 0520 UTC on 4 September. Time series of surface winds derived from (e) the meteorological model (CTL), (f) the parametric TC model (CTL), and (g) MSM at Osaka Port. One full wind barb is 50 $m \cdot s^{-1}$. The typhoon positions, central pressure, and radius of maximum wind used in Para-Jebi were based on the results of WRF-Jebi. The maximum wind and radius of maximum wind for Para-Jebi were detected by the axisymmetric mean tangential winds.

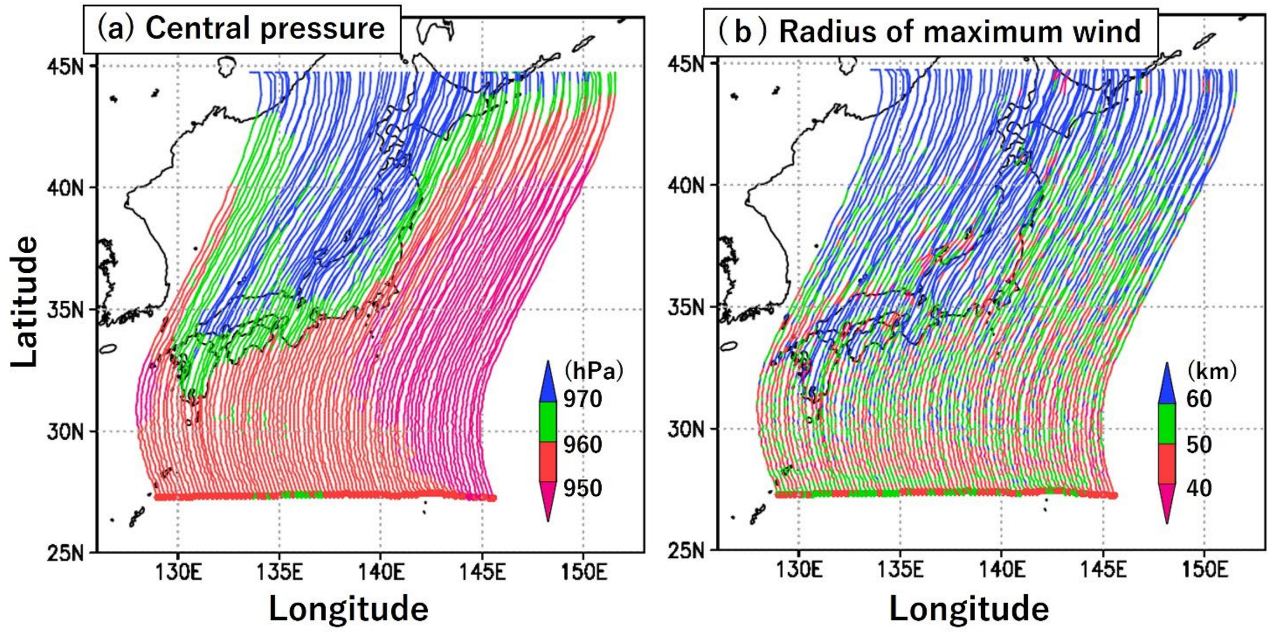

Figure 5: Tracks of Typhoon Jebi simulated by WRF ensemble experiments showing the (a) central pressure and (b) radius of maximum wind of Typhoon Jebi.

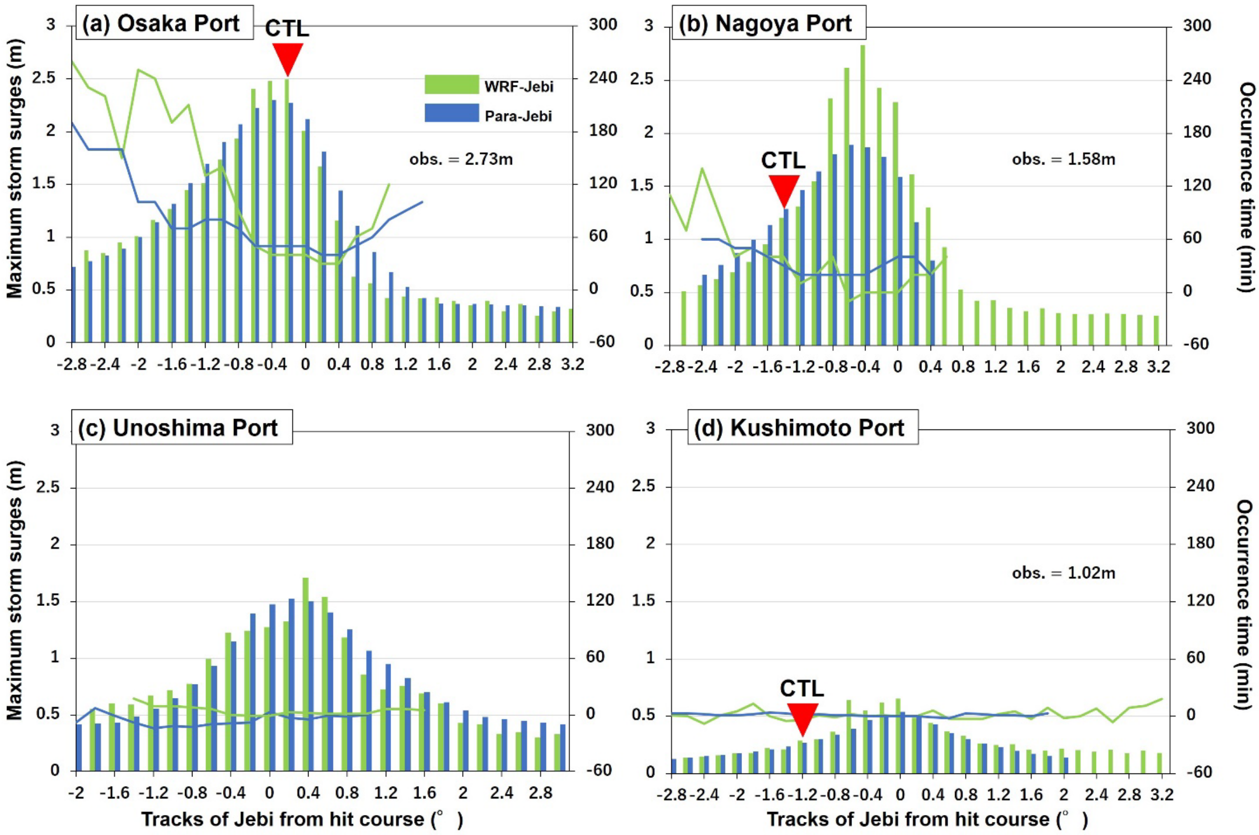

Figure. 6: Maximum storm surge (bar) and occurrence time (line) for various tracks of Typhoon Jebi relative to the hit course at (a) Osaka Port, (b) Nagoya Port, (c) Unoshima Port, and (d) Kushimoto Port. Plots were derived from the JMA storm surge model, with Typhoon Jebi simulated by the meteorological (green) and parametric TC (blue) models. The red triangle indicates the CTL, which is 3.4° to the east of the hit course for Unoshima Port. The observed maximum storm surges are shown in the graph, excluding Unoshima.

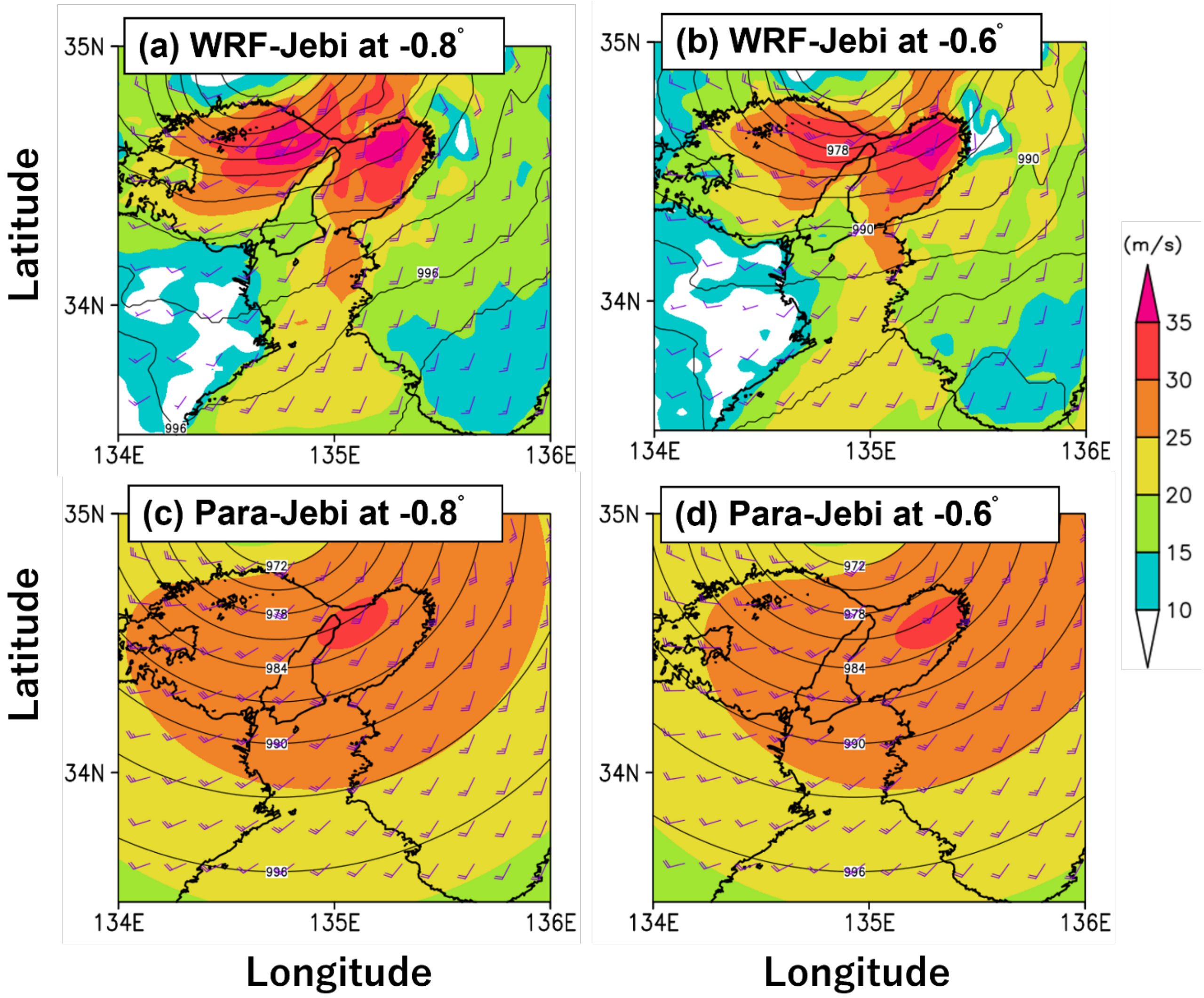

Figure 7: Surface winds at 10 m height (wind barbs, a full wind barb represents $m \cdot s^{-1}$.), wind speeds (shaded), and sea-level pressure (contour, contour interval is 3 hPa) simulated by (a) (b) the meteorological model and (c) (d) the parametric TC model at 0530 UTC on 4 September 2018, at (a) (c) 0.8° and (b) (d) 0.6° west of the hit course for Osaka Port.

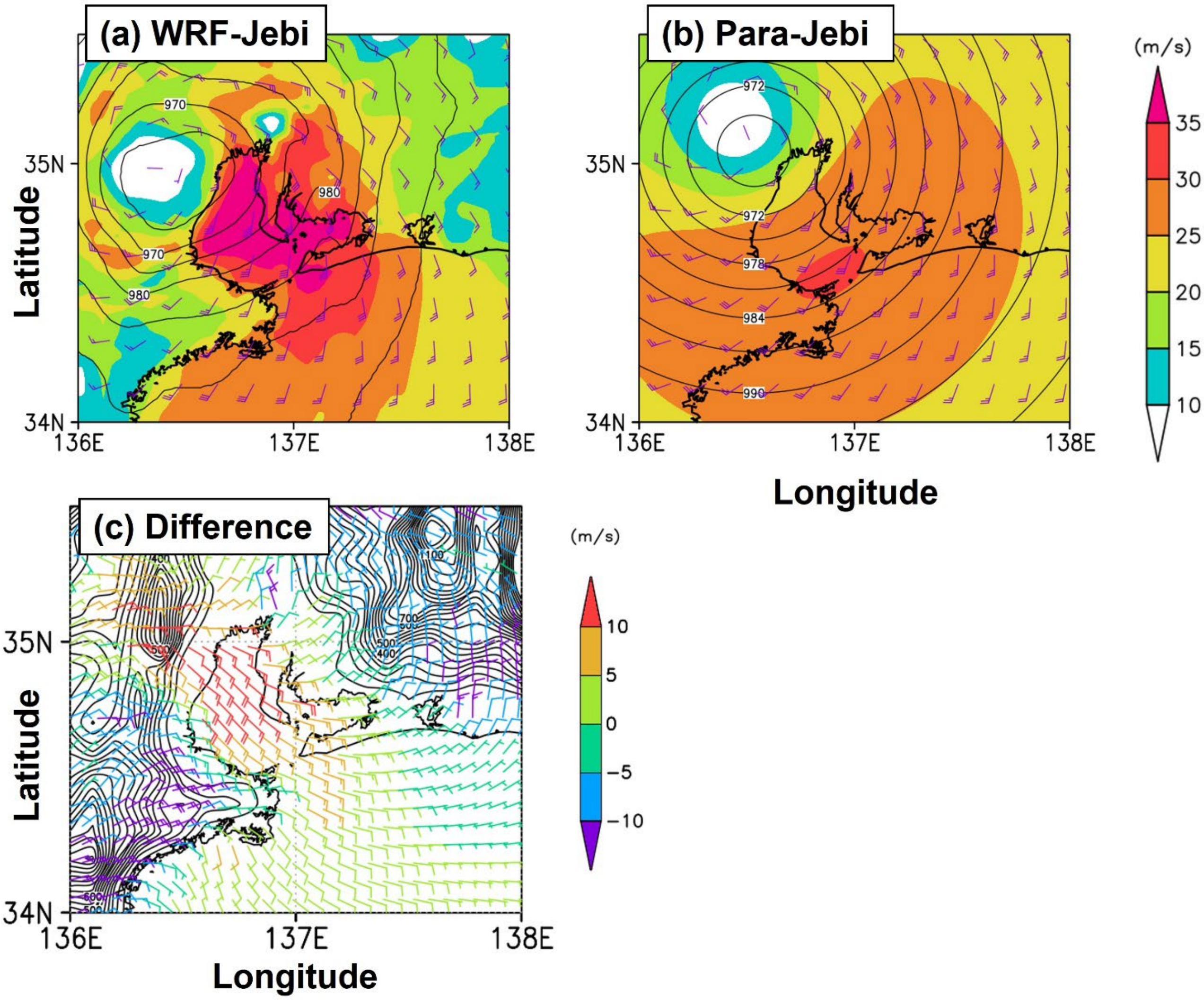

Figure 8: Surface winds at 10 m height (wind barbs, a full wind barb represents 50 m·s^{-1}.), wind speeds (shaded), and sea-level pressure (contour, contour interval is 3 hPa) simulated in (a) the meteorological model and (b) the parametric TC model at 0530 UTC on 4 September (the timing of the maximum storm surge), 0.4° west of the hit course for Nagoya Port. (c) The difference between WRF-Jebi and Para-Jebi surface wind at 0530 UTC on 4 September.

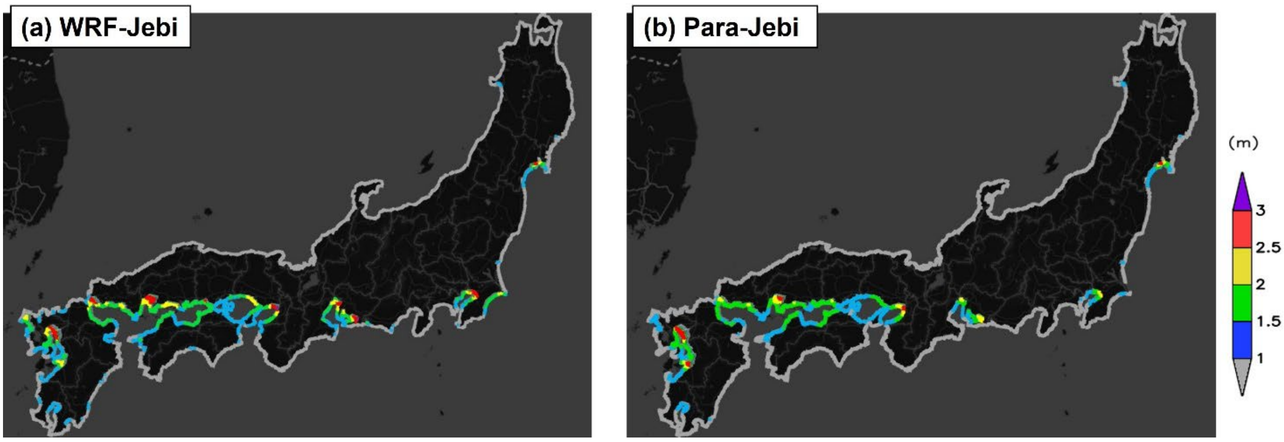

Figure 9: Maps of the maximum storm surges derived from the JMA storm surge model, with Typhoon Jebi simulated by (a) the meteorological model and (b) the parametric TC model.

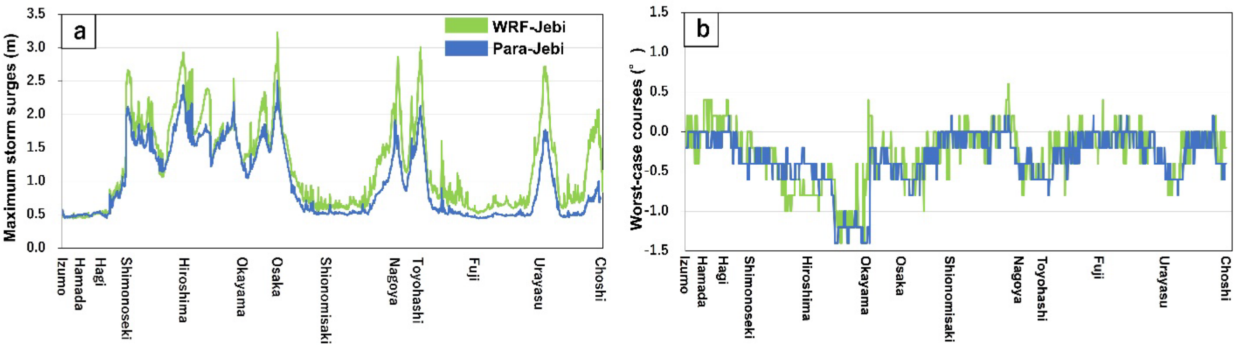

Figure 10: (a) Maximum storm surges and (b) the worst-case courses in coastal areas from Izumo to Choshi. Lines are derived from the JMA storm surge model, with Typhoon Jebi simulated by the meteorological (green) and parametric TC (blue) models.